Peptides 99 (2018) 169–178

Contents lists available at ScienceDirect

Peptides

journal homepage: www.elsevier.com/locate/peptides

Structure, folding and stability of a minimal homologue from *Anemonia sulcata* of the sea anemone potassium channel blocker ShK

Bankala Krishnarjuna[a], Christopher A. MacRaild[a], Punnepalli Sunanda[b], Rodrigo A.V. Morales[a], Steve Peigneur[c], Jason Macrander[d,e], Heidi H. Yu[f], Marymegan Daly[d], Srinivasarao Raghothama[b], Vikas Dhawan[g], Satendra Chauhan[g], Jan Tytgat[c], Michael W. Pennington[g], Raymond S. Norton[a,*]

[a] *Medicinal Chemistry, Monash Institute of Pharmaceutical Sciences, Monash University, 381 Royal Parade, Parkville, VIC 3052, Australia*
[b] *NMR Research Centre, Indian Institute of Science, Bangalore 560012, India*
[c] *Toxicology and Pharmacology, University of Leuven, O & N 2, Herestraat 49, P.O. Box 922, 3000, Leuven, Belgium*
[d] *Department of Evolution, Ecology, Organismal Biology, Ohio State University, 1315 Kinnear Rd, Columbus, OH 43212, USA*
[e] *Department of Biology, University of North Carolina at Charlotte, 9201 University City Blvd, Charlotte, NC 28223, USA*
[f] *Infection and Immunity Program, Monash Biomedicine Discovery Institute and Department of Microbiology, Monash University, VIC 3800, Australia*
[g] *Peptides International, Louisville, KY 40299, USA*

ARTICLE INFO

Keywords:
Cysteine-rich peptide
Sea anemone
K_V channel
NMR spectroscopy
Structure

ABSTRACT

Peptide toxins elaborated by sea anemones target various ion-channel sub-types. Recent transcriptomic studies of sea anemones have identified several novel candidate peptides, some of which have cysteine frameworks identical to those of previously reported sequences. One such peptide is AsK132958, which was identified in a transcriptomic study of *Anemonia sulcata* and has a cysteine framework similar to that of ShK from *Stichodactyla helianthus*, but is six amino acid residues shorter. We have determined the solution structure of this novel peptide using NMR spectroscopy. The disulfide connectivities and structural scaffold of AsK132958 are very similar to those of ShK but the structure is more constrained. Toxicity assays were performed using grass shrimp (*Palaemonetes* sp) and *Artemia nauplii*, and patch-clamp electrophysiology assays were performed to assess the activity of AsK132958 against a range of voltage-gated potassium (K_V) channels. AsK132958 showed no activity against grass shrimp, *Artemia nauplii*, or any of the K_V channels tested, owing partly to the absence of a functional Lys-Tyr dyad. Three AsK132958 analogues, each containing a Tyr in the vicinity of Lys19, were therefore generated in an effort to restore binding, but none showed activity against any of K_V channels tested. However, AsK132958 and its analogues are less susceptible to proteolysis than that of ShK. Our structure suggests that Lys19, which might be expected to occupy the pore of the channel, is not sufficiently accessible for binding, and therefore that AsK132958 must have a distinct functional role that does not involve K_V channels.

1. Introduction

Sea anemones are venomous animals that belong to the phylum Cnidaria and class Anthozoa [1]. They have tentacles surrounding their mouth and each tentacle bears specialized venomous organelles called nematocysts [1,2], which are used to capture food (prey) and defend against predators [1,3]. Sea anemone venoms are a rich source of disulfide-containing peptides [4] with molecular masses 3–6 kDa [2,5,6], many of which are active against various ion channels as inhibitors or modulators [6].

Peptides with the same cystine framework generally exhibit similar structural scaffolds [7], although they may or may not have the same biological function [7]. Peptides may show the same biological function if the relative orientation of the functionally important amino acid residues is conserved in their structures [8]. For example, a dyad that is formed by Lys and Tyr residues is key to potassium channel blockade by the sea anemone peptides ShK (from *Stichodactyla helianthus*) and BgK (from *Bunadosoma granulifera*), in which these amino acid residues are sequential, and by structurally distinct scorpion peptides such as charybdotoxin [9,10] and HsTX1 [11], in which the amino acid residues are distant from each other in sequence but close in space [8,12–14]. Therefore, the activity is mostly dependent on the key amino acid residues and their orientation in relation to the rest of the molecule rather than the structural scaffold on which they are presented.

ShK blocks the voltage-gated potassium channel $K_V1.3$ with low pM affinity [8,12]. As $K_V1.3$ is expressed on human effector memory T

* Corresponding author.
E-mail address: ray.norton@monash.edu (R.S. Norton).

http://dx.doi.org/10.1016/j.peptides.2017.10.001
Received 7 July 2017; Received in revised form 3 October 2017; Accepted 5 October 2017
Available online 06 October 2017
0196-9781/

lymphocytes (T_{EM}) and regulates their activation and proliferation [15], selective inhibition of this channel is an effective strategy to treat autoimmune diseases. An analogue of ShK is currently under development for the treatment of autoimmune diseases such as psoriasis [16–18]. The ShK fold first observed in this peptide [19] is widely distributed in nature, occurring not only in sea anemones and other coelenterates, but also in parasitic worms and higher organisms [20–22]. While many members of this ShK family may be potassium channel blockers, other functions have already been observed [22] and others will no doubt be identified in future.

Genomic and transcriptomic studies on sea anemones have led to a rapid increase in the identification of novel peptide sequences [23–26]. Through our transcriptomic study of *Anemonia sulcata,* we identified a sequence coding for a peptide with an ShK-like cystine framework. This peptide was of interest as it contains only 29 amino acid residues with six half-cystines, and was identical to ShK in only 12 positions, six of which were half-cystines. We were interested to determine if this peptide could indeed adopt an ShK-like fold, and whether it had the ability to block potassium channels even though it lacked an obvious Lys-Tyr dyad. We therefore solved the solution structure of AsK132958 and designed analogues based on its structural similarities with ShK and BgK, in an effort to engineer activity against $K_V1.3$ and closely-related K^+ channels.

2. Materials and methods

2.1. Identification of peptide

Candidate ShK-like genes were identified using previously characterized ShK-like peptides (Fig. 1) as sequence queries against previously published sea anemone transcriptomes [21]. Candidate ShK-like transcripts were translated into their protein sequences in Geneious [27] and further evaluated via reciprocal BLAST against the non-redundant protein database on NCBI. Candidate ShK toxins were aligned using MAFFT v7.017 [28] to ensure that the structural cysteine residues were present in each candidate transcript. The MAFFT alignment used an automatic algorithm selection, BLOSUM 62 scoring matrix, 1.8 gap open penalty, and 0.123 offset value. The ShK-like sequence in *A. sulcata* was assigned the number 132958 by Geneious [27]. The systematic name, U-ASTX-Asu1, is derived from the nomenclature proposed by Oliveira et al. [29]. The protein sequence alignment was used to reconstruct gene trees for ShK-like genes. The maximum likelihood gene tree reconstruction was carried out in the program PHYML [30] using the WAG substitution model with 1000 bootstrap replicates. The program MrBayes [31] was used to reconstruct Bayesian ShK-like gene trees with four heated chains at a temp of 0.2, subsampled every 200 replicates over a chain length of 1,000,000 after a burn-in length of 100,000. The tree and alignments were visualized in Geneious [27].

2.2. Peptide synthesis

AsK132958 and each of the Tyr-substituted analogues were synthesized using *N*-(9-fluorenyl) methoxycarbonyl (Fmoc)-Cys(Trt)-Wang resin on a Prelude automated peptide synthesizer (Protein Technologies, Tucson, Arizona). All couplings were mediated with diisopropylcarbodiimide with 6-chloro-1-hydroxybenzotriazole (6-Cl-HOBT) for 3 h. Following removal of the final Fmoc protecting group, each of the peptides was cleaved from the resin support and simultaneously deprotected using a cocktail of trifluoroacetic acid, anisole, triisopropylsilane, thioanisole, H_2O and 1,2 ethanedithiol (9:1:2:1:1:1 v/v) for 2 h at room temperature. The crude peptides were precipitated and washed three times with ice-cold diethyl ether, then subsequently dissolved in 50% aqueous acetic acid and diluted into H_2O to a concentration of 0.3 mg/mL. The pH of the peptide solution was adjusted to 7.8 with ammonium hydroxide (NH_4OH). Disulfide bond formation was accelerated by addition of 0.1 mM glutathione (reduced and oxidized) and the peptide solution was stirred gently for 18 h. The crude folded peptide was purified by reversed-phase high-performance liquid chromatography (HPLC) on a Phenomenex® Luna C18 column (100 Å, 5 μm, 100 × 10 mm) using a gradient of 10–50% acetonitrile vs 0.05% TFA in H_2O over 20 min with absorbance monitored at 220 nm. The fractions were analysed using analytical HPLC using the same gradient conditions. The purity and molecular mass of each peptide was confirmed by electrospray ionisation mass spectroscopy (ESI–MS). The pure fractions were pooled and lyophilized. Based upon the starting resin substitution, the yield for each of the peptides was nearly 35%.

2.3. NMR spectroscopy

Samples for NMR experiments were prepared by dissolving lyophilized peptides in 95% H_2O/5% ^2H_2O and adjusting the pH to 4 by adding 0.1 M NaOH. The sample for deuterium exchange experiments was prepared by dissolving AsK132958 in 100% ^2H_2O and the pH was adjusted to 4 using 0.1 M ^2HCl or 0.1 M NaO^2H.

NMR spectra were acquired on 600 and 800 MHz Bruker NMR spectrometers equipped with cryogenically cooled triple-resonance probes. Two-dimensional [^1H-^1H] total correlation spectroscopy (2D TOCSY) (50 and 80 ms mixing times) and 2D [^1H-^1H] nuclear Overhauser effect spectroscopy (NOESY) experiments (50–250 ms mixing times) were recorded in phase-sensitive mode using states-TPPI for quadrature detection in the indirect dimension. A DIPSI2 sequence was used for isotropic mixing in the 2D TOCSY [32]. The experiments were acquired with 400 and 2048 complex data points in t_1 and t_2 dimensions, respectively. TOCSY and NOESY were recorded with 32 and 88 scans, respectively, per increment. One-dimensional (1D) ^1H spectra were recorded at different temperatures ranging from 10 to 40 °C, at intervals of 10 °C. Similarly, 2D TOCSY spectra with a spin lock time of

Fig. 1. MAFFT alignment and maximum likelihood Shk-like gene tree reconstruction. When applicable, branch labels include Genbank ID, toxin name, and species. Circles indicate support values for branches, with ≫ > 50 bootstrap (BS) for maximum likelihood having the first half of the circle filled and branches with ≫ > 0.85 posterior probability (PP) values having the second half of the circle filled in. Amino acid residues present in greater than 50% of the amino acid sequences in the alignment are highlighted. The two ShK-like transcripts from *Heteractis crispa* are indicated with an asterisk.

80 ms and NOESY spectra with a mixing time of 250 ms were acquired at 20, 30 and 40 °C for resolving overlapped spin systems. TOCSY and NOESY were recorded using an excitation sculpting pulse scheme [33] and DQF-COSY was recorded using a Watergate pulse scheme [34] for H_2O suppression. The 2D data were zero-filled to 8192 and 4096 t_1 and t_2 points respectively and then processed using a sine-bell squared window function before Fourier transformation. ^{1}H-^{13}C and ^{1}H-^{15}N heteronuclear single-quantum coherence (HSQC) spectra (with sensitivity enhancement scheme) [35] were recorded in phase-sensitive mode using echo-antiecho for quadrature detection in the indirect dimension. All spectra were processed in Bruker TopSpin 3.2 and analysed using CcpNmr Analysis (Version 2.4) [36,37]. 1,4-Dioxane at 3.75 ppm was used for calibrating the ^{1}H dimension, and the ^{13}C and ^{15}N dimensions were calibrated indirectly. Temperature coefficients were calculated from amide proton chemical shifts (obtained from 2D TOCSY spectra acquired at different temperatures) to predict the hydrogen bond donors [38]. The pH titrations were performed using 2D TOCSY spectra over the pH range 2–5; the pH of the sample was measured before and after each acquisition. The complete list of ^{1}H and ^{15}N chemical shifts has been deposited in the BioMagResBank [39] database (BMRB ID: 30315).

2.4. Structural restraints and structure calculation

The structure of AsK132958 was calculated using internuclear distances from NOESY spectra, dihedral angles estimated from $^{3}J_{HNH\alpha}$ coupling constants and hydrogen bonds predicted from amide proton exchange rates and temperature coefficients. A total of 494 NOE-derived distances was converted into unambiguous structural restrains. Initial structures were calculated by CYANA [40] (version 3.97) using only NOE distance constraints. Three-bond $^{3}J_{HNH\alpha}$ coupling constants were measured from 1D ^{1}H or DQF-COSY spectra; seven φ angles were restrained to $-120 \pm 40°$ when $^{3}J_{HNH\alpha} \geq 8$ Hz and $-65 \pm 25°$ when $^{3}J_{HNH\alpha} \leq 6$ Hz. Three χ1 angles obtained from DQF-COSY and NOESY spectra [41] were also included as restraints. Three distance constraints were used for disulfide connectivities as follows: 2, 3 and 3 Å for S(i)-S(j), S(i)–Cβ(j), and S(j)–Cβ(i), respectively. Amide proton exchange rates and temperature coefficients, donor-acceptor distances, together with hydrogen bond acceptors predicted from initial structure calculations (present and consistent in ≥ 80% of structures), were used to predict hydrogen bonds and these were included as restraints in subsequent structure calculations. The structures generated using CYANA were refined by simulated annealing, first *in vacuo*, then in implicit solvent using the EEFx force field in XPLOR-NIH (version 2.45) [42]. It was necessary to increase the force constants on angle and improper terms within the EFFx force field in order to obtain acceptable covalent geometry in this system. Ramachandran statistics were generated using Molprobity Ramachandran analysis in protein structure validation suite version 1.5 [43]. All the structure figures were generated using PyMOL (http://www.pymol.org).

2.5. Voltage-clamp electrophysiology

AsK132958 activity against various K^+ channels was tested using patch-clamp electrophysiology assays. For expression of voltage-gated potassium channels ($rK_V1.1$, $rK_V1.2$, $hK_V1.3$, $rK_V1.4$, $rK_V1.5$, $rK_V1.6$, Shaker IR, $rK_V4.2$, hERG, $hK_V10.1$) in *Xenopus* oocytes, the linearized plasmids were transcribed using the T7 or SP6 mMESSAGE-mMACHINE transcription kit (Ambion, Waltham, MA, USA). The harvesting of stage V–VI oocytes from anaesthetized female *Xenopus laevis* frog has been described previously [44]. Oocytes were injected with 30–50 nL of cRNA at a concentration of 1 ng/nL using a micro-injector (Drummond Scientific, Broomall, PA, USA). The oocytes were incubated in a solution containing (in mM): NaCl, 96; KCl, 2; CaCl2, 1.8; MgCl2, 2 and HEPES, 5 (pH 7.4), supplemented with 50 mg/L gentamycin sulfate.

Two-electrode voltage-clamp recordings were performed at room temperature (18–22 °C) using a GeneClamp 500 amplifier (Molecular Devices, Silicon Valley, CA, USA) controlled by a pClamp data acquisition system (Axon Instruments, Union City, CA, USA). Whole cell currents from oocytes were recorded 1–10 days after injection. Bath solution composition was ND96 (in mM): NaCl, 96; KCl, 2; $CaCl_2$, 1.8; $MgCl_2$, 2 and HEPES, 5 (pH 7.4). Voltage and current electrodes were filled with 3 M KCl. Resistances of both electrodes were kept between 0.8 and 1.5 mΩ. The elicited currents were sampled at 1 kHz and filtered at 0.5 kHz (for potassium currents) using a four-pole low-pass Bessel filter. Leak subtraction was performed using a −P/4 protocol. The $K_V1.1$–$K_V1.6$ and $K_V4.2$ and Shaker IR currents were evoked by 250 ms depolarizations to 0 mV followed by a 250 ms pulse to −50 mV, from a holding potential of −90 mV. Current traces of hERG channels were elicited by applying a pulse from −90 mV to +40 mV for 2.5 s followed by a step to −120 mV for 2.5 s. The $K_V10.1$ currents were evoked by 1 s depolarization to 0 mV, from a holding potential of −90 mV. All data represent independent experiments (n = 3 for all AsK132958 and n = 6 for ShK).

2.6. Whole organism assay

Grass shrimp (*Palaemonetes* sp.) were collected nearshore in Clambake Creek, South Carolina, USA (33.341° and −79.193°) on May 9, 2017. The shrimp were maintained for 1 month in flow-through aquaria on a 12 h:12 h light/dark cycle prior to AsK132958 assays. AsK132958 and each of its analogues were injected at a concentration of 25 ng per 100 mg of shrimp into the ventral side of three shrimp each. The shrimp remained under observation for 24 h. A follow-up experiment for AsK132958 and its analogues was done for three shrimp at a concentration of 500 ng per 100 mg of shrimp. Following similar procedures, injections of ShK were used as a positive control for neurotoxic activity at 25 ng and 250 ng per 100 mg of shrimp. Injections of 1 μL of water from aquaria per 100 mg of shrimp served as a negative control. Brine shrimp (*Artemia nauplii*) were also used as a lethality assay for AsK132958 and ShK. Brine shrimp were hatched in artificial salt water at 30 PPT and collected after 24 h. Approximately ten *Artemia nauplii* were placed into three culture plates and acclimated for 30 min prior to adding AsK132958 or ShK at a final concentration of 250 ng/μL.

2.7. Antimicrobial activity assay

Peptide stocks were prepared in Milli-Q water at 1 mg/mL and filter-sterilised through 0.22 μm filter. Each peptide at 10 μL and 50 μL volumes was transferred onto a blank 6 mm (diameter) disc (Oxoid), then placed onto 0.5-McFarland-matched swab cultures of *Pseudomonas aeruginosa* (ATCC 27853), *Acinetobacter baumannii* (ATCC 19606), *Klebsiella pneumoniae* (ATCC 700721), *Escherichia coli* (ATCC 25922) and *Staphylococcus aureus* (ATCC 43300). Milli-Q water and colistin were used as controls. Plates were incubated at 37 °C for 24 h and the zones of inhibition were measured (diameter) in millimeters as per Clinical and Laboratory Standards Institute (CLSI) guidelines.

2.8. Proteolysis assay

Proteolysis assays were performed with trypsin (EC 3.4.21.4), α-chymotrypsin (EC 3.4.21.1) and pepsin (EC 3.4.23.1), at 250:1 peptide/enzyme ratio. Enzyme stocks were prepared at 100 μM concentration. Trypsin and chymotrypsin were prepared in 50 mM Tris (pH 7.4) buffer containing 100 mM NaCl and 2 mM $CaCl_2$, and pepsin was prepared in 10 mM HCl (pH 2). The reactions for trypsin and α-chymotrypsin were performed in 50 mM Tris-HCl (pH 7.4) buffer containing 100 mM NaCl and 2 μM $CaCl_2$. The reaction for pepsin was performed in 1 mM HCl (pH 2). Peptides (25 μM) were incubated with enzyme at 37 °C and the reaction was monitored and analysed by liquid chromatography–mass spectrometry (LC–MS) (0–60% acetonitrile gradient, 10 min) after 0,

0.5, 1, 2, 4, 6, 8 and 16 h of incubation. Trypsin and α-chymotrypsin reactions were quenched by addition of 1% TFA, and the pepsin reaction was quenched by addition of 200 mM ammonium acetate (pH 7.4). ShK and contryphanVc1 were used as control substrates in proteolysis assays.

3. Results

3.1. ShK-like identification and gene tree reconstruction

Of the ShK-like transcripts identified in our previous transcriptomic study (Fig. 1) AsK132958 had the lowest level of sequence identity when compared to other ShK-like peptides and was one of the shortest. Although there were two additional ShK-like amino acid sequences identified in *Heteractis crispa*, only one of them retained the Lys-Tyr dyad (Fig. 1). Additionally, two new ShK-like amino acid sequences were identified during the reciprocal BLAST search for *Exaiptasia pallida* and *Nematostella vectensis*, both lacking the Lys-Tyr dyad. Collectively, these ShK-like transcripts, along with AsK132958, highlighted the substantial variation that exists in anemone ShK-like genes and remains to be evaluated functionally.

Both tree reconstruction methods resulted in trees with relatively low support values throughout. The differences between trees are in parts of the tree with particularly low support. The protein sequence alignment revealed that there is a greater incidence of variation in the 5′ region upstream from the cleavage site when compared to the mature peptide region. For AsK132958 the entire predicted amino acid sequence looked very different from other ShK amino acid sequences, and it is the shortest evaluated thus far, being four amino acid residues shorter than κ-AITX-Aer3a and κ-SHTX-Hmg1a, both of which bind to voltage-gated K^+ channels [45,46].

3.2. Synthesis of AsK132958 and its analogues

ESI–MS results confirmed that AsK132958 was pure and its mass was correct as expected for the oxidised form of this peptide (Table S1 and Fig. S1). The peptide yield for AsK132958 after folding was higher than the ShK yield reported previously [47]. All three Tyr-containing analogues (see below) gave similarly good yields.

3.3. Sequence-specific resonance assignments

Initially, partial assignments were made using NMR spectra recorded at pH 5, but it was noticed that cross-peaks for the backbone amide proton of His17 were missing in these spectra owing to its fast-intermediate exchange with solvent protons. Therefore, spectra were recorded at pH 4 and 293 K (Figs. S2 and S3) and used for sequential assignments. 2D TOCSY and NOESY spectra recorded at different temperatures were used to resolve overlapped spin systems. Side-chain assignments were obtained from 2D DQF-COSY and TOCSY spectra. Stereospecific assignments were obtained from DQF-COSY and NOESY spectra (recorded with 50 ms mixing time) [41]. The chemical shifts of all ^1H and ^{15}N of AsK132958 are listed in Table S2 in Supplementary information. Slowly exchanging amides observed 8 h after dissolution of AsK132958 in 100% ^2H_2O and having temperature coefficients ≪4.5 ppb/K were considered for inclusion as hydrogen bond donors in structure calculations. The 2D ^1H-^{15}N HSQC spectrum with all the backbone assignments is shown in Fig. 2.

3.4. Disulfide bonds are well defined

Mass spectrometry and the Cα and Cβ chemical shifts of cysteines confirmed that AsK132958 contained three disulfide bonds (Table S3 and Fig. S1). The Cβ chemical shifts of all cysteines are ≫ > 35 ppm, indicating the formation of disulfide bonds [48]. Initial structures were calculated by CYANA using NOE constraints without defining the disulfide connectivities. The connectivities were clearly defined based on the proximity of cysteine residues in these initial structures, and were consistent with NOEs between the side-chains of cysteine residues (Table S3 and Fig. S4). Since Cys1 and Cys29 are on the surface and more flexible, we detected no NOEs for the Cys1-Cys29 pair.

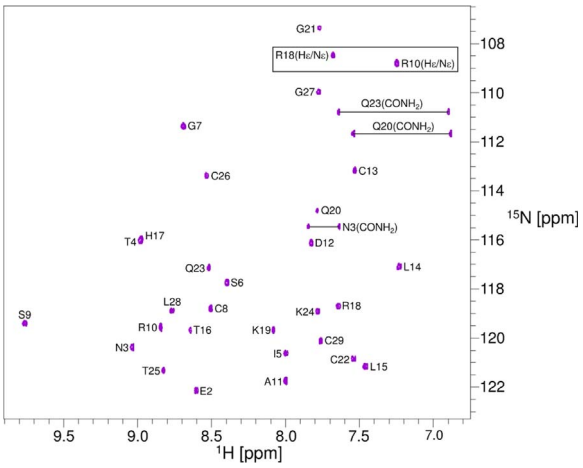

Fig. 2. Two-dimensional [^1H-^{15}N]-HSQC spectrum of AsK132958 with resonance assignments. The spectrum was acquired at 20 °C and pH 4 on a Bruker Avance III 600 MHz spectrometer. Folded peaks are boxed.

3.5. AsK132958 has ShK-like structural scaffold

Fig. 3A shows a stereo view of the final ensemble of 20 lowest energy structures from 100 structures refined in implicit solvent using XPLOR-NIH. The structures are well defined, with backbone and heavy atom RMSD values over all amino acid residues of 0.37 and 0.77 Å, respectively. The longer side chains of a few charged amino acid residues have increased RMSD (Fig. S5). The structural ensemble has been deposited in the Protein Data Bank [49] (PDB ID: 5WCV).

AsK132958 has two short helices spanning amino acid residues 10–14 and 23–26. The first nine amino acid residues at the N-terminus adopt an extended conformation lacking any turns. The 3_{10} helix spanning amino acid residues 10–14 is stabilized by a 13 → 10 hydrogen bond as well as the flanking half-cystine residues at positions 8 and 13. There is a loop region between Leu15 and Arg18, which is followed by a weak helical turn encompassing Lys19 to Gly21. This helical turn is stabilized by a 22 → 18 hydrogen bond. The loop region includes His17, the backbone amide of which is in fast-intermediate exchange with solvent protons at pH above 4, suggesting that the loop region is solvent exposed. A helix spanning amino acid residues 23–26 is present at the C-terminus and is stabilized by a 28 → 23 hydrogen bond. Fig. S6 shows resonances of slowly exchanging amide protons that were considered as H-bond donors in structure calculations. The 20 best structures show that 99.8% of amino acid residues were in the most favoured and 0.2% in additionally allowed regions of a Ramachandran plot (Table 1). No distance restraints or dihedral angle restraints were violated. Fig. 3B shows a stereo view of the closest-to-average structure of AsK132958 highlighted with helices, turns, a loop region and disulfide bonds. Overall AsK132958 has an ShK-like structural scaffold with the same disulfide bond connectivity (Fig. 3C). It was proposed in ShK that electrostatic interactions between Asp5 and Lys30 were crucial for efficient oxidative folding of the peptide [19,50]. In AsK132958, Glu2 and Lys24 are close in proximity (the distances between Glu2 Oε and Lys24 Nζ; range from 4.1 to 10.0 Å in 20 structures) suggesting similar electrostatic interactions between them (Fig. S7). The p*K*a of Glu2 in AsK132958 measured from the pH dependence of its H^N resonance was 3.6 (Fig. S8), indicating a stabilization of the ionized form of this residue, consistent with an electrostatic interaction with a nearby positive charge. Moreover, NOEs were observed between

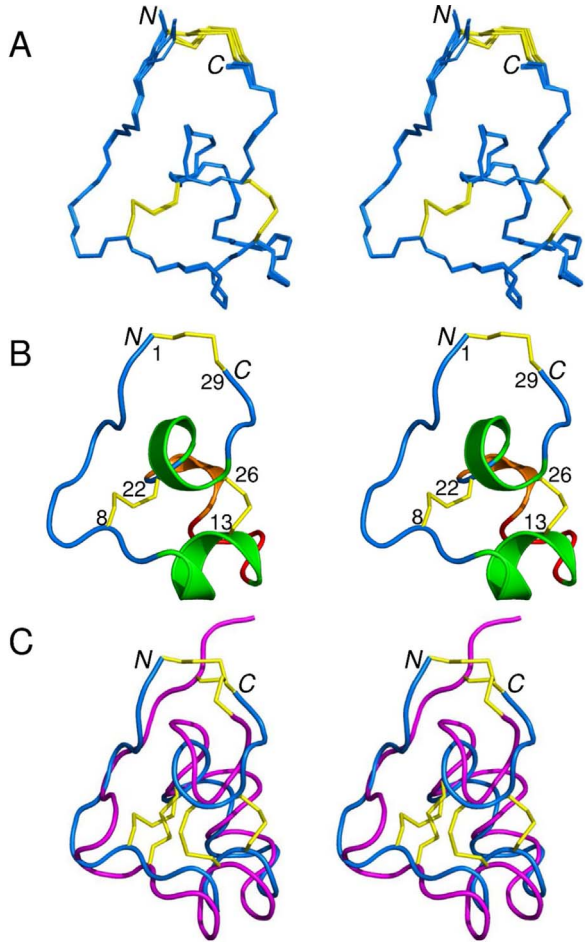

Fig. 3. (A) Stereo view (cross-eyed) of the best 20 structures of AsK132958, superimposed over the backbone heavy atoms N, Cα and C for amino acid residues 1–29. Only the backbone heavy atoms are shown, except for the three disulfide bonds (C1-C29, C8-C22 and C13-C26), which are coloured yellow. (B) Stereo view (cross-eyed) of backbone and closest-to-average structures of AsK132958. Helices are coloured green, the helical turn is coloured orange and loop region is red. (C) Stereo view (cross-eyed) of AsK132958 structure (blue, PDB id 5WCV) overlayed with ShK solution structure (magenta, PDB id 1roo). Disulfide bonds are displayed in yellow. N and C indicate N- and C-termini, respectively.

Table 1
NMR restrains and structure statistics for AsK132958.

NMR restrains	
Total NOEs	494
Intra-residue	110
Inter-residue	
Sequential	115
Medium-range	120
Long-range	149
Hydrogen bonds	3
Total dihedral angles	10
Backbone (ϕ angle)	7
Sidechain (χ1 angle)	3
Structure statistics	
NOE RMSD (Å)	0.042
Dihedral RMSD (Å)	0.488
Total number of violations	0
RMSD between 20 conformers (amino acid residues 2–29)	
Average pairwise RMSD (Å)	
Backbone (Å) (N, Cα, C)	0.183
All heavy atoms (Å)	0.846
Ramachandran analysis	
Amino acid residues in most favoured regions (%)	99.8
Amino acid residues in additionally allowed regions (%)	0.2

```
A AsK      --CENTIS--GCS----RADC--LLTHRKQGCQKTCGLC
  ShK      RSCIDTIPKSRCT----AFQCKHSMKYRLSFCRKTCGTC
  BgK      -VCRDWFKETACRHAKSLGNCRTSQKYR-ANCAKTCELC
             *        *        *      *   * ***  *

B ChTX      ZFTNVSCTTSKECWSVCQRLHNTSRGKCMNKKCRCYS-
  Vm24      -AAAISCVGSPECPPKCR-AQGCKNGKCMNRKCKCYYC
  HsTX1     ----ASCRTPKDCADPCRKETGCPYGKCMNRKCKCNRC
               **     *   *        ***** ** *
```

Fig. 4. Amino acid sequences of sea anemone and scorpion peptide toxins. (A) Sequence alignment of closely related sea anemone (AsK132958, ShK and BgK) and (B) scorpion (ChTX, Vm24 [from *Vaejovis mexicanus*] and HsTX1) peptide toxins. Functional residues of Lys-Tyr dyad are underlined in all the amino acid sequences. Clustal Omega was used for sequence alignment.

backbone and sidechains of Glu2 and Lys24 residues in the 2D NOESY. The presence of these NOEs further supports an interaction between Glu2 and Lys24 residues, which may contribute to the efficient folding and stability of AsK132958.

3.6. AsK132958 and analogues showed no activity in functional assays

A functional Lys-Tyr dyad is usually required for the activity of K_V1.3 peptide blockers [8,51]. In the amino acid sequences of closely-related sea anemone peptides such as ShK and BgK, the Lys and Tyr residues of the dyad are sequential (Fig. 4A). In the scorpion peptide toxins, the functional amino acid residues are not sequential (Fig. 4B), although they are close (6–7 Å) in space [8,52]. Although AsK132958 lacks a Lys-Tyr dyad, its activity against K_V channels was assessed.

AsK132958 was subjected to testing against a wide range of ion channels. The peptide was investigated on cloned voltage-gated potassium channels (K_V1.1–K_V1.6, K_V4.2, K_V10.1, hERG and Shaker IR) expressed in *X. laevis* oocytes. At concentrations up to 100 μM, this peptide showed no activity on the different K_V channel isoforms tested. It is possible that the lack of a Lys-Tyr functional dyad in AsK132958 may have been the reason for its lack of activity against K_V1.3. Therefore, AsK132958 analogues were designed based on the AsK132958 structure and the relative orientation of Lys and Tyr residues in sea anemone and scorpion peptide toxins (Fig. 4). Thr16, Gln20 and Leu28 surrounding Lys19 in AsK132958 were selected for replacement with a Tyr (Fig. 5). The distance between Cα of Lys19 and the plane of Tyr is 6–7 Å in the Q20Y analogue, which is similar to that in K_V1.3 blocking peptides such as ShK and BgK. This distance is

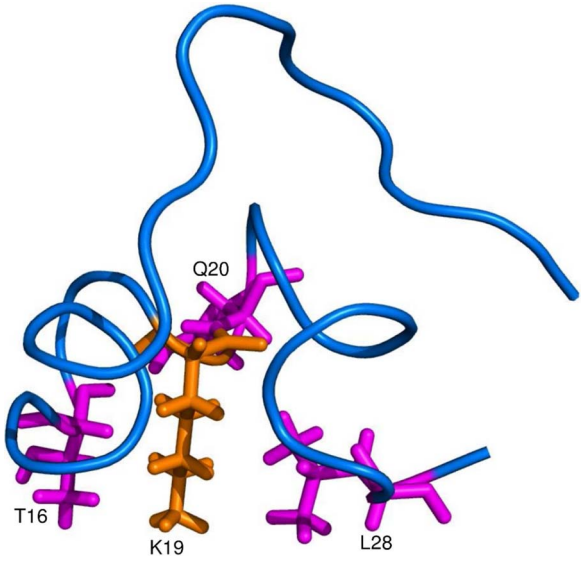

Fig. 5. AsK132958 amino acid residues selected for replacement with Tyr to create a possible Lys-Tyr dyad. Backbone is coloured blue, Lys19 is coloured orange and Thr16, Gln20 and Leu28 are coloured magenta. Disulfide bonds are omitted for clarity.

slightly longer, at about 8 Å, in the T16Y and L28Y analogues.

AsK132958 analogues were produced utilising the same protocols as for AsK132958. Mass spectroscopy confirmed that all analogues were fully oxidized. Well-resolved chemical shifts were observed in the ^{1}H-NMR spectra of AsK132958 analogues, confirming that all the peptides were well folded. Moreover, the chemical shift dispersion in these spectra was similar to that in the spectrum of AsK132958 (Fig. S9), indicating that the mutations did not affect the overall structure of AsK132958. These analogues were also subjected to testing against the same channels that were tested against AsK132958 at the same concentration. Unfortunately, none of the peptides showed activity on the different K_V channel isoforms tested. The control peptide ShK showed an IC50 of 50.3 ± 5.1 pM in these assays.

AsK132958 and its analogues were also subjected to testing for their toxicity using grass shrimp (*Palaemonetes* sp) and Brine shrimp (*Artemia nauplii*). Even when grass shrimp and Brine shrimp were subjected to concentrations exceeding what is considered a lethal dose in other sea anemone toxins [53], the organismal assays showed 100% survival for all treatments, including ShK injections for grass shrimp and exposures for *Artemia nauplii*. At 500 ng per 100 mg of shrimp there were no noticeable immediate or long-term neurotoxic effects after 24 h that would differentiate AsK-injected shrimp from negative controls. ShK injections induced immediate neurotoxic effects, with noticeable twitching of legs at 25 ng/100 mg of shrimp. The symptoms were exaggerated at 250 ng per 100 mg of shrimp. After 24 h the ShK-injected shrimp did not exhibit any neurotoxic symptoms.

AsK132958 and its analogues were also tested for their efficacy in inhibiting bacterial growth. None of the AsK132958 peptides showed growth inhibitory activity against any bacteria tested. *P. aeruginosa* ATCC 27853 and *E. coli* ATCC 25922 were employed as quality control strains and their colistin zones of inhibition were within the CLSI guideline range.

3.7. AsK132958 and its analogues are less susceptible to proteolysis than ShK

Proteolytic stability is an important property in developing peptides into drug candidates. We therefore examined the stability of AsK132958 and its analogues in the presence of three proteolytic enzymes (trypsin, chymotrypsin and pepsin) and compared this with the stability of ShK (Figs. 6 and S10–S15).

Trypsin, which cleaves peptides on the C-terminal side of Lys and Arg residues, was able to digest all peptides tested, albeit at distinct rates (Figs. 6 A, S10 and S12–14). AsK132958 and its T16Y analogue had half-lives of over 3 h in the presence of trypsin (Figs. 6 A and S12). The L28Y analogue was more susceptible to trypsin, with a half-life of 2 h, and was completely digested in 16 h (Figs. 6 A and S13). Interestingly, the Q20Y analogue was four-fold more resistant than AsK132958, with a half-life of 16 h (Figs. 6 A and S14). ShK had the shortest half-life (0.5 h) of all peptides tested and was completely digested within 6 h (Fig. 6A).

Chymotrypsin (which cleaves on the C-terminal side of hydrophobic amino acid residues, preferably aromatic amino acid residues) did not cleave AsK132958 over 16 h, whereas it completely digested ShK within 8 h (Figs. 6 B and S10). Interestingly, the Q20Y and L28Y AsK132958 analogues were also not affected by chymotrypsin (Figs. 6 B, S13 and S14) despite having a cleavable site at Tyr, suggesting that this cleavable site may be partly buried in their structures. The T16Y AsK132958 analogue, containing Tyr in the flexible loop, was digested up to 65% in the first 2 h and slowly reached 70% in 16 h of incubation (Figs. 6 B and S12). LC–MS data indicated that the proteolysis led to the accumulation of a stable peptide population of the T16Y analogue carrying a single internal hydrolysed site (Fig. S15). The accumulated nicked T16Y may be reducing the rate of hydrolysis by competing with non-digested T16Y for binding with chymotrypsin. ShK was completely digested within 8 h (Figs. 6 B and S11).

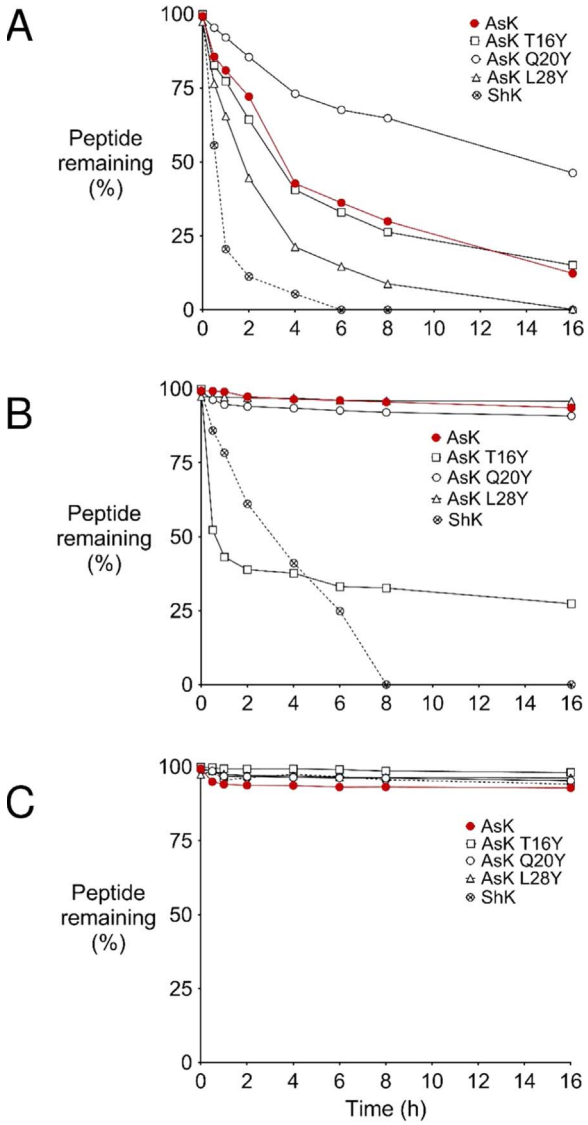

Fig. 6. Stability of AsK132958 and its analogues upon treatment with proteolytic enzymes (A) trypsin, (B) chymotrypsin and (C) pepsin at 37 °C. Plot was derived from the peak area determined by liquid chromatography–mass spectrometry. ShK peptide was used as a control.

The stability of these peptides was also tested in the presence of pepsin, which cleaves peptide bonds N-terminal to aromatic amino acid residues. AsK132958 was not digested by pepsin owing to the absence of any aromatic amino acid residues in its sequence (Figs. 4 A and 6 C). Surprisingly, neither ShK nor AsK132958 analogues which have one or more aromatic amino acid residues, was affected by pepsin (Figs. 6 C and S12–14). The activity of pepsin was confirmed using the reduced form of the single-disulfide containing peptide contryphan Vc1 [54] (Fig. S16).

4. Discussion

In this study we have characterized a novel ShK-like peptide, AsK132958, which was identified in a transcriptomic study of *Anemonia sulcata*. Although AsK132958 is shorter (29 amino acid residues) than ShK, we obtained correctly folded AsK132958 without any difficulty and in fact the final yield of AsK132958 was higher than that of ShK. AsK132958 is a slightly basic peptide (pI 7.8) although less so than ShK (pI 9.5). Previous reports of the failure of oxidative refolding of ShK mutants in which Asp5 was replaced by Asn or Lys30 by Ala implied

that electrostatic or hydrogen bonding interactions, which are important for peptide folding and stability [50,55], might be present between Asp5 and Lys30 in ShK. The corresponding amino acid residues in AsK132958, Glu2 and Lys24, in AsK132958 may have a similar role. The N−O distances between Glu2 and Lys24 side-chains in AsK132958 and Asp5 and Lys30 in solution structures of ShK vary from 4.1 to 10.0 Å and 2.3–8.5 Å, respectively (Fig. S7). Although an N−O distance of less than 4 Å [56–58] is typical of a salt-bridge, the variation of this parameter across the ensemble of NMR structures of both AsK132958 and ShK may be consistent with more dynamic, long-range electrostatic interactions [59]. The low pKa of Glu2 (3.6) supports the existence of these weak interactions (Figs. S7 and S8). In this study, we have not tested the mutational effect of any amino acid residues on the efficacy of oxidative folding of AsK132958.

Structural analyses of peptide toxins that block K_V1.3 channels have suggested that a functional dyad containing a Lys residue and an aromatic (Tyr or Phe) or hydrophobic (Leu) residue is crucial for their activity [8,13]. Although K_V1.3-blocking scorpion peptides are structurally different from sea anemone peptides, they mostly also have a conserved functional dyad [13]. The distance between Cα of Lys and the plane of Tyr in the structures of K_V1.3-blocking peptides such as ShK, BgK1, ChTX and Vm24 is around 6–7 Å [8,52]. Lys22, which is on the surface of ShK [19,60] (Fig. 7), protrudes into the pore region of the K_V1.3 channel upon binding [61–64]. Tyr23 in ShK is not as exposed as Lys22, and in fact NMR relaxation dispersion measurements detect some flexibility in the region of the dyad, which may enhance the exposure of Tyr23 and facilitate channel binding [65,66]. AsK132958 is six amino acid residues shorter than ShK, with two of the extra amino acid residues in ShK lying between the first two cysteines and another two between the third and fourth cysteines (Fig. 4A). Owing to the short inter-cysteine regions, the AsK132958 structure is more constrained than ShK (Fig. 3C). While AsK132958 has two Lys residues, at positions 19 and 24 (Fig. 4A), Lys24 is involved in an interaction with Glu2, leaving Lys19 as the only residue potentially able to interact with the K_V channel.

AsK132958 showed no activity against a range of voltage-gated potassium channels, or brine shrimp or grass shrimp in this work. Although some peptides from other species [67] share sequence similarity with ShK, they are inactive against K_V1 channels owing to the lack of a Lys-Tyr dyad in their structures. AsK132958 appears to be one such peptide. Based on the sequence alignment of AsK132958, ShK and BgK (Fig. 4A), we predicted that it may be possible to form a Lys-Tyr dyad by introducing a Tyr at specific sites in AsK132958, and thereby generate activity against K_V channels. Hence, Q20Y, T16Y and L28Y were prepared and tested against a series of potassium channels, but none of them were active. Similarly, none of these peptides exhibited any antimicrobial activity against the range of bacterial strains tested in this work. Our structure shows that Lys19 in AsK132958 is not as exposed as Lys22 in ShK or Lys25 in BgK and Vm24 (Figs. 5 and 7), and this is probably the major contributor to the lack of inhibition of Kv channels. Moreover, Tyr in our AsK132958 analogues may be oriented differently from the dyad Tyr in these peptides. Both of these factors are likely to disfavour binding to K_V channels. Superposition of the structures of AsK132958 and ShK (Fig. 8A) suggests that the loop region between Leu15 and Arg18 in AsK132958 may be a suitable location to introduce a Lys-Tyr dyad (eg. in place of His17-Arg18) (Fig. 8B) to generate an active AsK132958 analogue. Some scorpion peptides, such as BmP02 and BmP03 (from *Mesobuthus martensii*), Tc32 (from *Tityus cambridgei*) and Kbot1 (from *Buthus occitanus*), are active against K_V1.3 with nM affinities even though they lack functional dyads [68–71]. BmP02, for example, uses a cluster of three basic amino acid residues to inhibit K_V1.3 [72]. AsK132958 contains neither a dyad as in ShK/BgK

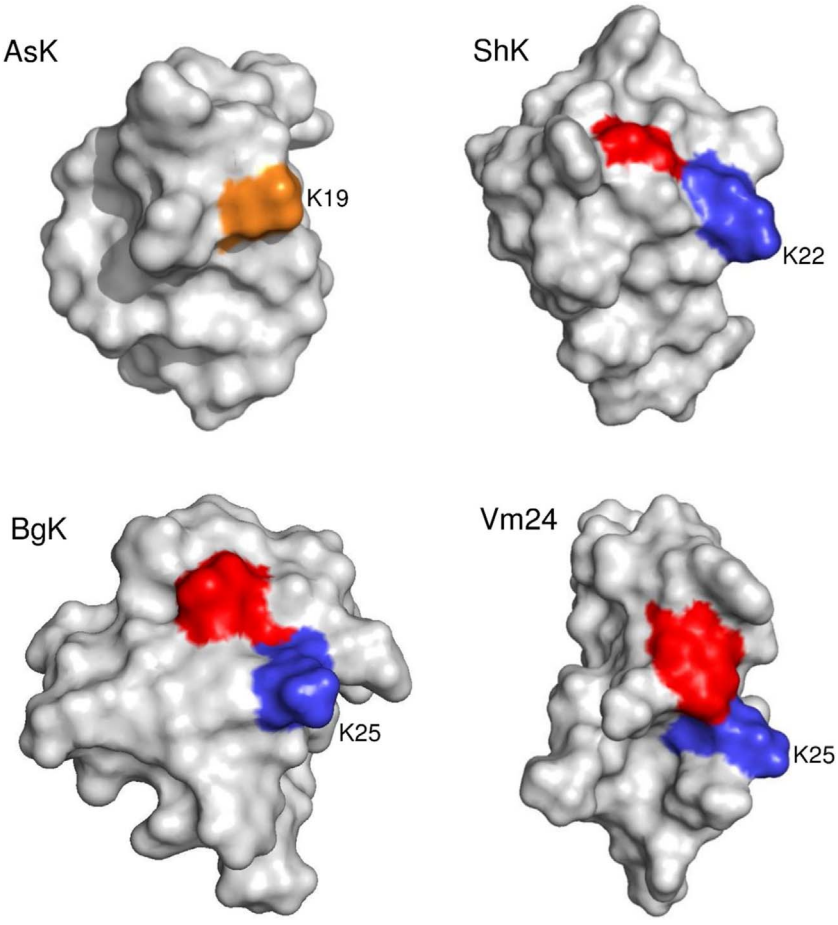

Fig. 7. Surface representation of AsK132958 (PDB ID: 5WCV), ShK (PDB ID: 1roo), BgK (PDB id 1bgk) and Vm24 (PDB id 2k9o). In each structure the functional dyad containing a Lys (blue) and a Tyr (red) is highlighted. An equivalent Lys in the AsK132958 is coloured orange. In AsK132958, the Lys is less exposed on the surface than in ShK, BgK and Vm24, which all block K_V1.3.

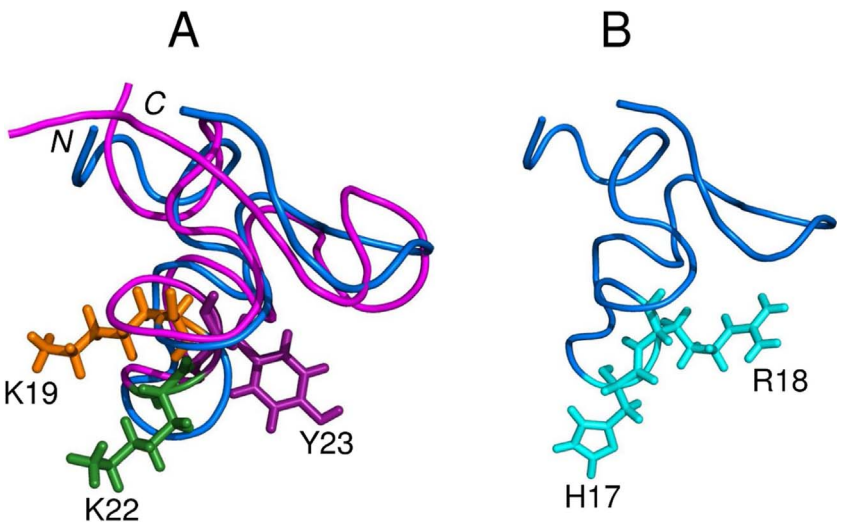

Fig. 8. (A) Overlay of structures of AsK132958 (blue) (PDB id 5WCV) and ShK (magenta) (PDB id 1roo) highlighting Lys19 (orange) in the AsK132958 and the Lys22 (green) −Tyr23 (purple) dyad in the ShK. (B) The loop region (amino acid residues L15-R18) of AsK132958 (cyan) showing the side chains of His17 and Arg18. Disulfides are omitted for clarity. N and C indicate N- and C-termini, respectively.

nor other functionally important residues as in BmP02 (Fig. S17). Our sequence alignment (Fig. 1) revealed that there are five other ShK-like amino acid sequences that lack this Lys-Tyr dyad, but none of these have been functionally characterized as yet.

It is possible that the functionally important Lys-Tyr dyad residues were incorporated into ShK-like scaffolds with strong directional selection pressures resulting in the acquisition of neurotoxic functions. Given the relatively low support values in our tree, it is difficult to determine whether all ShK-like peptides are members of the same gene family. In light of the high rate of variation observed in the signalling region and prevalence of this domain in other non-venomous animals, we believe it unlikely that all of the ShK-like genes we have identified are orthologous sequences. Thus, AsK132958 and other ShK-like amino acid sequences may have completely different evolutionary origins or biological roles from ShK.

When compared with ShK, the structure of AsK132958 is more constrained, has fewer positively charged (Lys and Arg) residues, and lacks aromatic amino acid residues (Fig. 4A). Therefore, AsK132958 is less susceptible to proteolysis by trypsin and chymotrypsin than ShK [73] (Fig. 6A and B). Similarly, AsK132958 analogues are less susceptible to trypsin, and in fact the Q20Y analogue is more resistant than AsK132958 itself (Fig. 6A). The increased susceptibility of the L28Y analogue to trypsin compared to AsK132958 and the other two analogues suggested increased accessibility of tryptic cleavage sites in this analogue. However, the replacement of the polar Gln20 with a Tyr residue partially reduced the access of potential tryptic cleavage sites (Arg18 and Lys19) without hindering the resistance of the peptide against chymotrypsin. The susceptibility of the T16Y analogue to hydrolysis by chymotrypsin is expected, as Tyr16 is within a flexible region (Figs. 5 and 6 B). The resistance of the Q20Y and L28Y analogues to chymotrypsin (Figs. 6 B, S13 and S14) suggests that the Tyr residues at these positions are significantly less exposed and, consequently, not available for chymotrypsin cleavage. This is consistent with our observation that they failed to form functional Lys-Tyr dyads.

AsK132958 is resistant to pepsin, owing to a lack of aromatic amino acid residues (Figs. 4 A, 6 C and S10B). Surprisingly, neither AsK132958 analogues nor ShK are affected by pepsin (Figs. 6 C and S12–14). Our analysis suggests that molecules with a globular fold may not be prone to cleavage by pepsin, because the active site in pepsin is located in a deep cleft region (Fig. S10B).

5. Conclusions

The solution structure of the sea anemone peptide AsK132958 is similar to that of ShK, and has the same disulfide connectivity pattern. Electrophysiology assays indicate, however, that AsK132958 does not target voltage-gated potassium channels. AsK132958 analogues with a Tyr residue at three different positions, were also not active against K_V channels, probably because neither Lys19 nor the introduced Tyr residues were sufficiently solvent-exposed and flexible. The evolutionary relationship, and thus orthology, between AsK132958 and other ShK-like amino acid sequences is unclear. It is possible that AsK132958 could be an evolutionary precursor of peptides with ShK-like scaffold and activity, or it may represent a completely different class of amino acid sequences with different biological function.

Acknowledgements

B.K acknowledges support from the Monash University Postgraduate Publication Award. R.S.N acknowledges fellowship support from the Australian National Health and Medical Research Council. The authors would like to thank Remi Ketchum and Whitney Leach for collecting the grass shrimp. This work was supported in part by a grant from the Australian Research Council (LP150100621). The facilities provided by NMR Research Centre at IISc, supported by the Department of Science and Technology (DST), India, are gratefully acknowledged. JT is supported by the following grants: VS.055.15N (FWO Vlaanderen), IUAP 7/10 (Inter-University Attraction Poles Program, Belgian State, Belgian Science Policy). MD and JM are supported by US National Science Foundation awards DEB-1401014 and DEB-1257796. The authors thank Charles D. Schwieters for helpful discussion regarding structure refinement using XPLOR.

Appendix A. Supplementary data

Supplementary data associated with this article can be found, in the online version, at http://dx.doi.org/10.1016/j.peptides.2017.10.001.

References

[1] B. Frazão, V. Vasconcelos, A. Antunes, Sea anemone (Cnidaria, Anthozoa, Actiniaria) toxins: an overview, Mar. Drugs 10 (8) (2012) 1812–1851.
[2] T. Honma, K. Shiomi, Peptide toxins in sea anemones: structural and functional aspects, Mar. Biotechnol. (NY) 8 (2006) 1–10.
[3] D. Todaro, G.M. Watson, Force-dependent discharge of nematocysts in the sea anemone *Haliplanella luciae* (Verrill), Biol. Open 1 (6) (2012) 582–587.
[4] E. Deplazes, Molecular simulations of disulfide-rich venom peptides with ion channels and membranes, Molecules 22 (3) (2017) 362.
[5] V. Lavergne, P.F. Alewood, M. Mobli, G.F. King, The structural universe of disulfide-rich venom peptides, G.F. King (Ed.), Venoms to Drugs: venom as a source for the development of human therapeutics, Royal Society of Chemistry (2015) 37-79.
[6] R.S. Norton, Sea anemone venom peptides, in: A.J. Kastin (Ed.), Handbook of Biologically Active Peptides, Elsevier (Academic), San Diego, 2006, pp. 363–367.

[7] N.L. Van Der Weerden, M.A. Anderson, Plant defensins: common fold, multiple functions, Fungal Biol. Rev.. 26 (4) (2013) 121–131.

[8] M. Dauplais, A. Lecoq, J. Song, J. Cotton, N. Jamin, B. Gilquin, C. Roumestand, C. Vita, C.L.C. de Medeiros, E.G. Rowan, A.L. Harvey, A. Ménez, On the convergent evolution of animal toxins: conservation of a diad of functional residues in potassium channel-blocking toxins with unrelated structures, J. Biol. Chem. 272 (7) (1997) 4302–4309.

[9] W. Massefski, A.G. Redfield, D.R. Hare, C. Miller, Molecular structure of charybdotoxin, a pore-directed inhibitor of potassium ion channels, Science 249 (4968) (1990) 521–524.

[10] F. Bontems, C. Roumestand, P. Boyot, B. Gilquin, Y. Doljansky, A. Menez, F. Toma, Three-dimensional structure of natural charybdotoxin in aqueous solution by ^{1}H NMR, Eur. J. Biochem. 196 (1) (1991) 19–28.

[11] B. Lebrun, R. Romi-Lebrun, M.F. Martin-Eauclaire, A. Yasuda, M. Ishiguro, Y. Oyama, O. Pongs, T. Nakajima, A four-disulphide-bridged toxin, with high affinity towards voltage-gated K^{+} channels, isolated from *Heterometrus spinnifer* (Scorpionidae) venom, Biochem. J. 328 (Pt 1) (1997) 321–327.

[12] K. Kalman, M.W. Pennington, M.D. Lanigan, A. Nguyen, H. Rauer, V. Mahnir, K. Paschetto, W.R. Kem, S. Grissmer, G.A. Gutman, E.P. Christian, M.D. Cahalan, R.S. Norton, K.G. Chandy, ShK-Dap22, a potent Kv1. 3-specific immunosuppressive polypeptide, J. Biol. Chem. 273 (49) (1998) 32697–32707.

[13] S. Gasparini, B. Gilquin, A. Ménez, Comparison of sea anemone and scorpion toxins binding to Kv1 channels: an example of convergent evolution, Toxicon 43 (8) (2004) 901–908.

[14] R.S. Norton, K.G. Chandy, Venom-derived peptide inhibitors of voltage-gated potassium channels, Neuropharmacology (2017) (inpress).

[15] K.G. Chandy, T.E. Decoursey, M.D. Cahalan, C. McLaughlin, A.S. Gupta, Voltage-gated potassium channels are required for human T lymphocyte activation, J. Exp. Med. 160 (2) (1984) 369–385.

[16] V. Chi, M.W. Pennington, R.S. Norton, E. Tarcha, L. Londono, B. Sims-Fahey, S.K. Upadhyay, J.T. Lakey, S. Iadonato, H. Wulff, C. Beeton, K.G. Chandy, Development of a sea anemone toxin as an immunomodulator for therapy of autoimmune diseases, Toxicon 59 (4) (2012) 529–546.

[17] K.G. Chandy, R.S. Norton, Peptide blockers of Kv1.3 channels in T cells as therapeutics for autoimmune disease, Curr. Opin. Chem. Biol. 38 (2017) 97–107.

[18] E.J. Tarcha, C.M. Olsen, P. Probst, D. Peckham, E.J. Muñoz-Elías, J.G. Kruger, S.P. Iadonato, Safety and pharmacodynamics of dalazatide, a Kv1.3 channel inhibitor, in the treatment of plaque psoriasis: a randomized phase 1b trial, PLoS One 12 (7) (2017) e0180762.

[19] J.E. Tudor, P.K. Pallaghy, M.W. Pennington, R.S. Norton, Solution structure of ShK toxin, a novel potassium channel inhibitor from a sea anemone, Nat. Struct. Mol. Biol. 3 (4) (1996) 317–320.

[20] S. Rangaraju, K.K. Khoo, Z.-P. Feng, G. Crossley, D. Nugent, I. Khaytin, V. Chi, C. Pham, P. Calabresi, M.W. Pennington, R.S. Norton, K.G. Chandy, Potassium channel modulation by a toxin domain in matrix metalloprotease 23, J. Biol. Chem. 285 (12) (2010) 9124–9136.

[21] H.M. Nguyen, C.A. Galea, G. Schmunk, B.J. Smith, R.A. Edwards, R.S. Norton, K.G. Chandy, Intracellular trafficking of the K_V1.3 potassium channel is regulated by the prodomain of a matrix metalloprotease, J. Biol. Chem. 288 (9) (2013) 6451–6464.

[22] G.M. Gibbs, M.J. Scanlon, J. Swarbrick, S. Curtis, E. Gallant, A.F. Dulhunty, M.K. O'Bryan, The cysteine-rich secretory protein domain of Tpx-1 is related to ion channel toxins and regulates ryanodine receptor Ca^{2+} signaling, J. Biol. Chem. 281 (7) (2006) 4156–4163.

[23] J. Macrander, M. Broe, M. Daly, Tissue-specific venom composition and differential gene expression in sea anemones, Genome Biol. Evol. 8 (8) (2016) 2358–2375.

[24] A. Nicosia, T. Maggio, S. Mazzola, A. Cuttitta, Evidence of accelerated evolution and ectodermal-specific expression of presumptive BDS toxin cDNAs from *Anemonia viridis*, Mar. Drugs 11 (11) (2013) 4213–4231.

[25] M. Jouiaei, K. Sunagar, A. Federman Gross, H. Scheib, P.F. Alewood, Y. Moran, B.G. Fry, Evolution of an ancient venom: recognition of a novel family of cnidarian toxins and the common evolutionary origin of sodium and potassium neurotoxins in sea anemone, Mol. Biol. Evol. 32 (6) (2015) 1598–1610.

[26] I. Urbarova, B. Karlsen, S. Okkenhaug, O. Seternes, S.D. Johansen, Å. Emblem, Digital marine bioprospecting: mining new neurotoxin drug candidates from the transcriptomes of cold-water sea anemones, Mar. Drugs 10 (10) (2012) 2265.

[27] M. Kearse, R. Moir, A. Wilson, S. Stones-Havas, M. Cheung, S. Sturrock, S. Buxton, A. Cooper, S. Markowitz, C. Duran, T. Thierer, B. Ashton, P. Meintjes, A. Drummond, Geneious basic: An integrated and extendable desktop software platform for the organization and analysis of sequence data, Bioinformatics 28 (12) (2012) 1647–1649.

[28] K. Katoh, K. Misawa, K.-i. Kuma, T. Miyata, MAFFT: a novel method for rapid multiple sequence alignment based on fast Fourier transform, Nucleic Acids Res. 30 (14) (2002) 3059–3066.

[29] J.S. Oliveira, D. Fuentes-Silva, G.F. King, Development of a rational nomenclature for naming peptide and protein toxins from sea anemones, Toxicon 60 (4) (2012) 539–550.

[30] S. Guindon, O. Gascuel, A simple, fast, and accurate algorithm to estimate large phylogenies by maximum likelihood, Syst. Biol. 52 (5) (2003) 696–704.

[31] J.P. Huelsenbeck, F. Ronquist, MRBAYES: Bayesian inference of phylogenetic trees, Bioinformatics 17 (8) (2001) 754–755.

[32] A.J. Shaka, C.J. Lee, A. Pines, Iterative schemes for bilinear operators; application to spin decoupling, J. Magn. Reson. 77 (2) (1988) 274–293.

[33] T.L. Hwang, A.J. Shaka, Water suppression that works. Excitation sculpting using arbitrary wave-forms and pulsed-field gradients, J. Magn. Reson. A 112 (2) (1995) 275–279.

[34] M. Piotto, V. Saudek, V. Sklenář, Gradient-tailored excitation for single-quantum NMR spectroscopy of aqueous solutions, J. Biomol. NMR 2 (6) (1992) 661–665.

[35] A.G. Palmer, J. Cavanagh, P.E. Wright, M. Rance, Sensitivity improvement in proton-detected two-dimensional heteronuclear correlation NMR spectroscopy, J. Magn. Reson. 93 (1) (1991) 151–170.

[36] W.F. Vranken, W. Boucher, T.J. Stevens, R.H. Fogh, A. Pajon, M. Llinas, E.L. Ulrich, J.L. Markley, J. Ionides, E.D. Laue, The CCPN data model for NMR spectroscopy: development of a software pipeline, Proteins: Struct. Funct. Bioinf. 59 (4) (2005) 687–696.

[37] S.P. Skinner, B.T. Goult, R.H. Fogh, W. Boucher, T.J. Stevens, E.D. Laue, G.W. Vuister, Structure calculation, refinement and validation using CcpNmr Analysis, Acta Crystallogr. D Biol. Crystallogr. 71 (1) (2015) 154–161.

[38] N.J. Baxter, M.P. Williamson, Temperature dependence of ^{1}H chemical shifts in proteins, J. Biomol. NMR 9 (4) (1997) 359–369.

[39] E.L. Ulrich, H. Akutsu, J.F. Doreleijers, Y. Harano, Y.E. Ioannidis, J. Lin, M. Livny, S. Mading, D. Maziuk, Z. Miller, E. Nakatani, C.F. Schulte, D.E. Tolmie, R. Kent Wenger, H. Yao, J.L. Markley, BioMagResBank, Nucleic Acids Res. 36 (2008) D402–D408 Database issue.

[40] P. Güntert, Automated NMR structure calculation with CYANA, Methods Mol. Biol. (2004) 353–378.

[41] G. Wagner, W. Braun, T.F. Havel, T. Schaumann, N. Gō, K. Wüthrich, Protein structures in solution by nuclear magnetic resonance and distance geometry, J. Mol. Biol. 196 (3) (1987) 611–639.

[42] C.D. Schwieters, J.J. Kuszewski, N. Tjandra, G. Marius Clore, The Xplor-NIH NMR molecular structure determination package, J. Magn. Reson. 160 (1) (2003) 65–73.

[43] I.W. Davis, A. Leaver-Fay, V.B. Chen, J.N. Block, G.J. Kapral, X. Wang, L.W. Murray, W.B. Arendall III, J. Snoeyink, J.S. Richardson, D.C. Richardson, MolProbity: all-atom contacts and structure validation for proteins and nucleic acids, Nucleic Acids Res. 35 (Suppl_2) (2007) W375–W383.

[44] S. Peigneur, B. Billen, R. Derua, E. Waelkens, S. Debaveye, L. Béress, J. Tytgat, A bifunctional sea anemone peptide with Kunitz type protease and potassium channel inhibiting properties, Biochem. Pharmacol. 82 (1) (2011) 81–90.

[45] G.S. Gendeh, L.C. Young, C.L.C. de Medeiros, K. Jeyaseelan, A.L. Harvey, M.C.M. Chung, A new potassium channel toxin from the sea anemone *Heteractis magnifica*: isolation, cDNA cloning, and functional expression, Biochemistry 36 (38) (1997) 11461–11471.

[46] Y. Hasegawa, T. Honma, H. Nagai, M. Ishida, Y. Nagashima, K. Shiomi, Isolation and cDNA cloning of a potassium channel peptide toxin from the sea anemone *Anemonia erythraea*, Toxicon 48 (5) (2006) 536–542.

[47] M.W. Pennington, M.E. Byrnes, I. Zaydenberg, I. Khaytin, J. De Chastonay, D.S. Krafte, R. Hill, V.M. Mahnir, W.A. Volberg, W. Gorczyca, W.R. Kem, Chemical synthesis and characterization of ShK toxin: a potent potassium channel inhibitor from a sea anemone, Int. J. Pept. Protein Res. 46 (5) (1995) 354–358.

[48] D. Sharma, K. Rajarathnam, ^{13}C NMR chemical shifts can predict disulfide bond formation, J. Biomol. NMR 18 (2) (2000) 165–171.

[49] H. Berman, K. Henrick, H. Nakamura, Announcing the worldwide protein data bank, Nat. Struct. Mol. Biol. 10 (12) (2003) 980.

[50] M.W. Pennington, V.M. Mahnir, D.S. Krafte, I. Zaydenberg, M.E. Byrnes, I. Khaytin, K. Crowley, W.R. Kem, Identification of three separate binding sites on ShK toxin, a potent inhibitor of voltage-dependent potassium channels in human T-lymphocytes and rat brain, Biochem. Biophys. Res. Commun. 219 (3) (1996) 696–701.

[51] K.N. Srinivasan, V. Sivaraja, I. Huys, T. Sasaki, B. Cheng, T.K.S. Kumar, K. Sato, J. Tytgat, C. Yu, B.C.C. San, S. Ranganathan, H.J. Bowie, R.M. Kini, P. Gopalakrishnakone, κ-Hefutoxin1, a novel toxin from the scorpion *Heterometrus fulvipes* with unique structure and function: importance of the functional diad in potassium channel selectivity, J. Biol. Chem. 277 (33) (2002) 30040–30047.

[52] G.B. Gurrola, R.A. Hernández-López, R.C. Rodríguez de la Vega, Z. Varga, C.V.F. Batista, S.P. Salas-Castillo, G. Panyi, F. del Río-Portilla, L.D. Possani, Structure, function, and chemical synthesis of *Vaejovis mexicanus* peptide 24: A novel potent blocker of Kv1.3 potassium channels of human T lymphocytes, Biochemistry 51 (19) (2012) 4049–4061.

[53] C. Beeton, M.W. Pennington, R.S. Norton, Analogs of the sea anemone potassium channel blocker ShK for the treatment of autoimmune diseases, Inflamm. Allergy Drug Targets 10 (5) (2011) 313–321.

[54] B. Chittoor, B. Krishnarjuna, R.A.V. Morales, C.A. MacRaild, M. Sadek, E.W.W. Leung, S.D. Robinson, M.W. Pennington, R.S. Norton, The single disulfide-directed β-hairpin fold. dynamics, stability, and engineering, Biochemistry (2017).

[55] J.E. Tudor, M.W. Pennington, R.S. Norton, Ionisation behaviour and solution properties of the potassium-channel blocker ShK toxin, Eur. J. Biochem. 251 (1–2) (1998) 133–141.

[56] S. Kumar, R. Nussinov, Close-range electrostatic interactions in proteins, ChemBioChem 3 (7) (2002) 604–617.

[57] D.J. Barlow, J.M. Thornton, Ion-pairs in proteins, J. Mol. Biol. 168 (4) (1983) 867–885.

[58] H.R. Bosshard, D.N. Marti, I. Jelesarov, Protein stabilization by salt bridges: concepts, experimental approaches and clarification of some misunderstandings, J. Mol. Recognit. 17 (1) (2004) 1–16.

[59] S. Kumar, R. Nussinov, Relationship between ion pair geometries and electrostatic strengths in proteins, Biophys. J. 83 (3) (2002) 1595–1612.

[60] B. Dang, T. Kubota, K. Mandal, F. Bezanilla, S.B.H. Kent, Native chemical ligation at Asx-Cys, Glx-Cys: chemical synthesis and high-resolution X-ray structure of ShK toxin by racemic protein crystallography, J. Am. Chem. Soc. 135 (32) (2013) 11911–11919.

[61] M.D. Lanigan, M.W. Pennington, Y. Lefievre, H. Rauer, R.S. Norton, Designed peptide analogues of the potassium channel blocker ShK toxin, Biochemistry 40 (51) (2001) 15528–15537.

[62] M.H. Rashid, S. Kuyucak, Affinity and selectivity of ShK toxin for the K_V1 potassium channels from free energy simulations, J. Phys. Chem. B 116 (16) (2012) 4812–4822.
[63] M.H. Rashid, S. Mahdavi, S. Kuyucak, Computational studies of marine toxins targeting ion channels, Mar. Drugs 11 (3) (2013) 848–869.
[64] R. Chen, A. Robinson, D. Gordon, S.-H. Chung, Modeling the binding of three toxins to the voltage-gated potassium channel (Kv1.3), Biophys. J. 101 (11) (2011) 2652–2660.
[65] I. Sher, S.C. Chang, Y. Li, S. Chhabra, A.G. Palmer, R.S. Norton, J.H. Chill, Conformational flexibility in the binding surface of the potassium channel blocker ShK, ChemBioChem 15 (16) (2014) 2402–2410.
[66] E. Meirovitch, O. Tchaicheeyan, I. Sher, R.S. Norton, J.H. Chill, Structural dynamics of the potassium channel blocker ShK: SRLS analysis of ^{15}N relaxation, J. Phys. Chem. B 119 (49) (2015) 15130–15137.
[67] Y. Moran, M. Gurevitz, When positive selection of neurotoxin genes is missing, FEBS J. 273 (17) (2006) 3886–3892.
[68] L. Zhu, B. Gao, L. Luo, S. Zhu, Two dyad-free Shaker-type K^+ channel blockers from scorpion venom, Toxicon 59 (3) (2012) 402–407.
[69] B. Mahjoubi-Boubaker, M. Crest, R.B. Khalifa, M.E. Ayeb, R. Kharrat, Kbot1, a three disulfide bridges toxin from *Buthus occitanus tunetanus* venom highly active on both SK and K_V channels, Peptides 25 (4) (2004) 637–645.
[70] C.V.F. Batista, F. Gómez-Lagunas, R.C. Rodríguez de la Vega, P. Hajdu, G. Panyi, R. Gáspár, L.D. Possani, Two novel toxins from the Amazonian scorpion *Tityus cambridgei* that block Kv1.3 and *Shaker* B K^+-channels with distinctly different affinities, Biochim. Biophys. Acta Proteins Proteomics 1601 (2) (2002) 123–131.
[71] S. Mouhat, M. De Waard, J.-M. Sabatier, Contribution of the functional dyad of animal toxins acting on voltage-gated Kv1-type channels, J. Pept. Sci. 11 (2) (2005) 65–68.
[72] B. Wu, B.F. Wu, Y.J. Feng, J. Tao, Y.H. Ji, Mapping the interaction anatomy of BmP02 on $K_V1.3$ channel, 6 (2016) 29431.
[73] M.W. Pennington, C. Beeton, C.A. Galea, B.J. Smith, V. Chi, K.P. Monaghan, A. Garcia, S. Rangaraju, A. Giuffrida, D. Plank, G. Crossley, D. Nugent, I. Khaytin, Y. LeFievre, I. Peshenko, C. Dixon, S. Chauhan, A. Orzel, T. Inoue, X. Hu, R.V. Moore, R.S. Norton, K.G. Chandy, Engineering a stable and selective peptide blocker of the Kv1.3 channel in T lymphocytes, Mol. Pharmacol. 75 (4) (2009) 762–773.